Sensor and Simulation Notes

Note 430

December 1998

Multi-Channel Impulse Radiating Antennas with Polarization Diversity

Everett G. Farr and Leland H. Bowen
Farr Research, Inc.

Carl E. Baum and William D. Prather
Air Force Research Laboratory / Directed Energy Directorate

Abstract

We describe here the tri-IRA and quad-IRA, which are derived from earlier versions of Impulse Radiating Antennas. In these new designs, the aperture is divided into three, four, or more sections, in order to provide at least two receive channels and at least one transmit channel, all within a very compact structure. The two receive channels allow one to receive two orthogonal polarizations. This configuration will be useful when searching for mines using the so-called "vampire" radar signature. This signature is a characteristic of certain manmade objects in certain symmetry configurations. Such objects cannot scatter any cross-polarized field, whereas natural objects scatter a stronger cross-polarized field component. In this note, we analyze the radiated fields of the tri-IRA and quad-IRA. We optimize the feed impedance, and we build a model tri-IRA. This model is tested in various configurations, and compared to theory.

I. Introduction

The so-called "vampire" signature in scattering has been proposed by Baum as a method to locate plastic or metallic unexploded mines[1]. To make optimal use of this effect, an Ultra-Wideband (UWB) antenna is needed that allows one to transmit one polarization and receive two orthogonal polarizations. The multi-channel IRAs, including a tri-IRA and quad-IRA provide a compact solution to that problem in a single integrated antenna with multiple channels.

In this note we present the theory of operation of these antennas. We optimize the impedance, using a variety of figures of merit, for both the tri-IRA and quad-IRAs. We also provide data on an example of such an antenna, a tri-IRA with diameter of 0.914 meters (36 inches).

II. The Antenna and the UWB Radar System

In its most basic form, a UWB radar system consists of an impulse or step-function source, a pair of antennas, a computer, a limiter, and a digitizer. Such a system is sketched out in block-diagram form in Figure 2.1. The antennas should be sufficiently broadband and nondispersive to be capable of transmitting a sharp impulse. A good candidate for such a system is a reflector IRA [2-4], which consists of a parabolic dish with four conical feed arms.
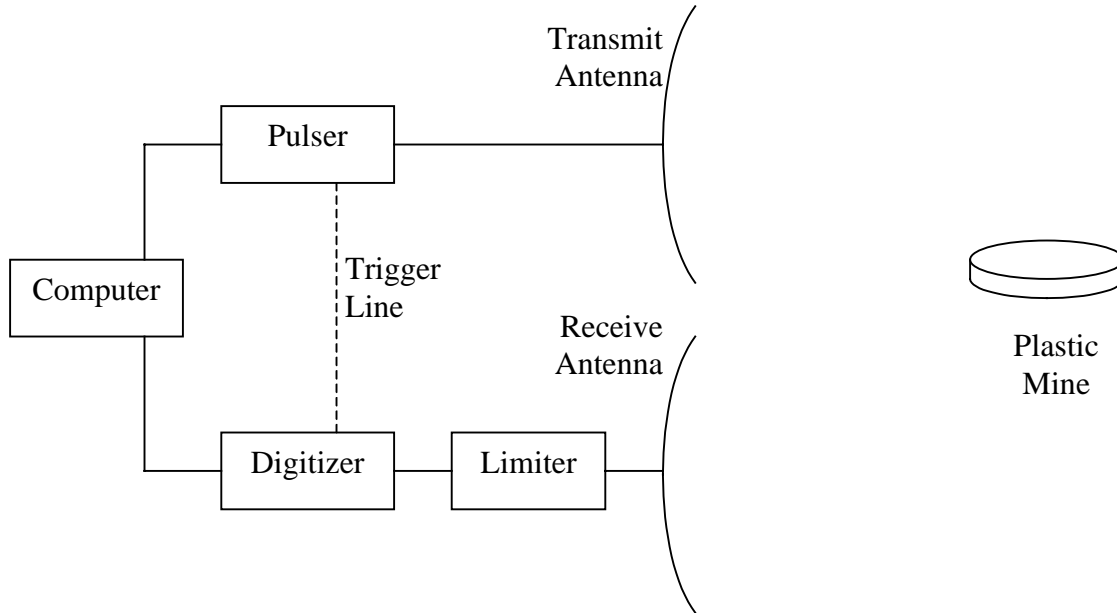

Figure 2.1. A UWB radar system.

In [1], Baum shows that a rotationally symmetry mine, sitting parallel to an air/soil interface, can scatter only co-polarized fields, and not cross-polarized fields. If we wish to use this effect to discriminate between mines and clutter, we will require an antenna that provides at least two of the four polarizations in the scattering dyadic.

One way to achieve this polarization diversity is with the tri-IRA, as shown in Figure 2.2. The reflector is split into three sections, with three ground planes separating the dish into separate channels. Each channel, referred to as a third-IRA, has two feed arms, forming an impedance of around 80 ohms. Note that Figure 2.2 shows only the projection of the feed in the aperture plane. Feed arms actually begin at the focus of the reflector and expand toward the outside edge of the reflector, as shown later in Figures 5.2 and 5.3. One of the antenna channels transmits vertical polarization, and the other two channels receive. By adding or subtracting the two receive channels, one gets either vertical or horizontal polarization. This is a very inexpensive way to obtain two of the four polarizations in the scattering dyadic, HH, VV, HV, and VH. To obtain the other two polarizations one could use a second tri-IRA rotated by 90 degrees. Note that HV = VH due to reciprocity.

An alternative method of getting all four polarizations in the scattering dyadic is to use a quad-IRA, as shown in Figure 2.3. In this configuration, there are four channels, two vertical and two horizontal. Each channel is referred to as a quarter-IRA. One channel of each polarization can be used for transmit and receive.
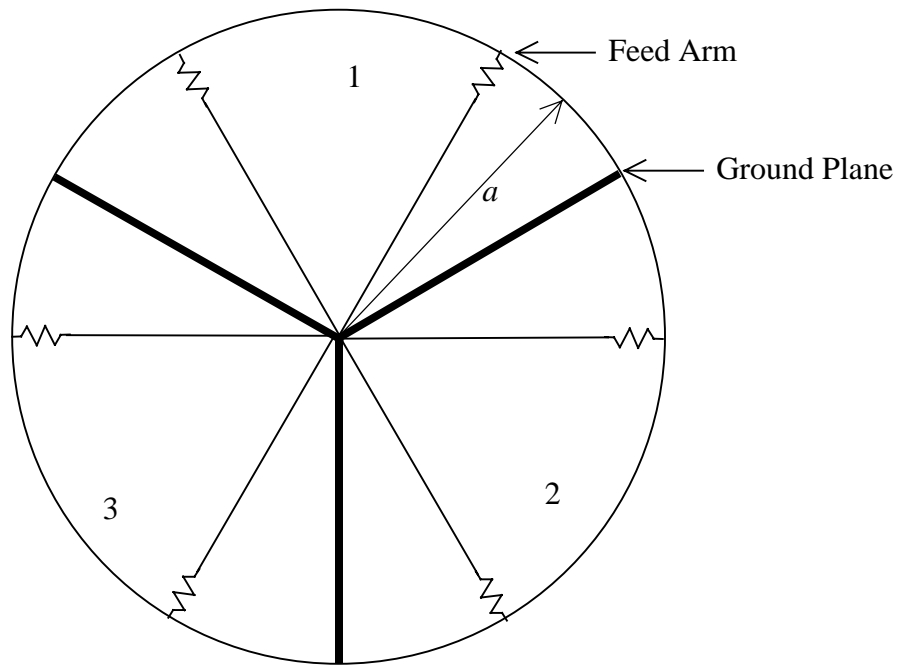
Figure 2.2. A tri-IRA. Channel 1 could transmit V, and H and V could be constructed from the sum and difference of channels 2 and 3.
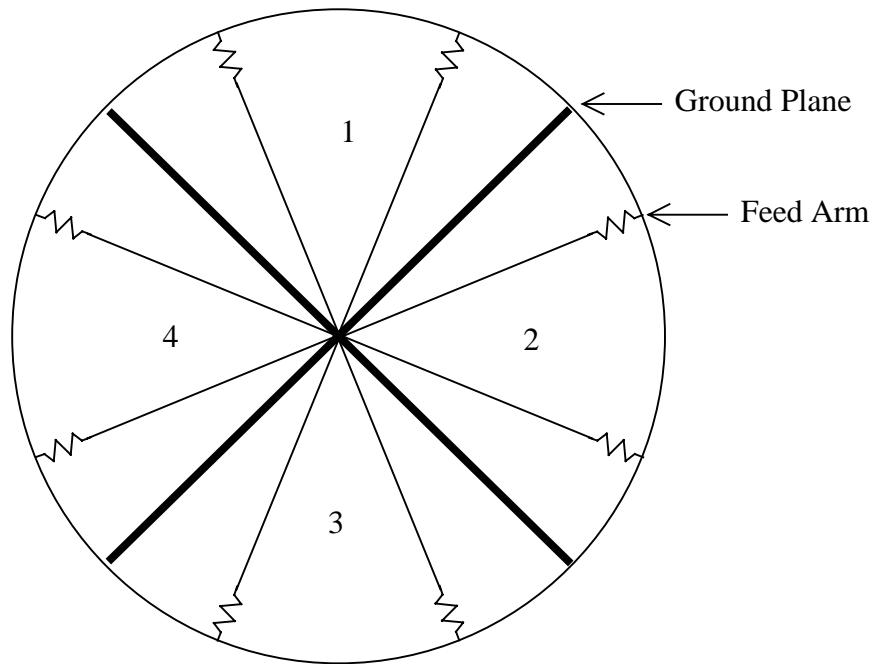

Figure 2.3. A quad-IRA. Channels 1 and 2 could transmit V and H, and Channels 3 and 4 could receive V and H.

When designing a tri-IRA, there may be some advantage to having the transmitting sector use half the aperture area, and the two receive channels each use one-quarter of the aperture. This design is shown in Figure 2.4. One might also say this design is a tri-IRA consisting of a half-IRA and two quarter-IRAs.
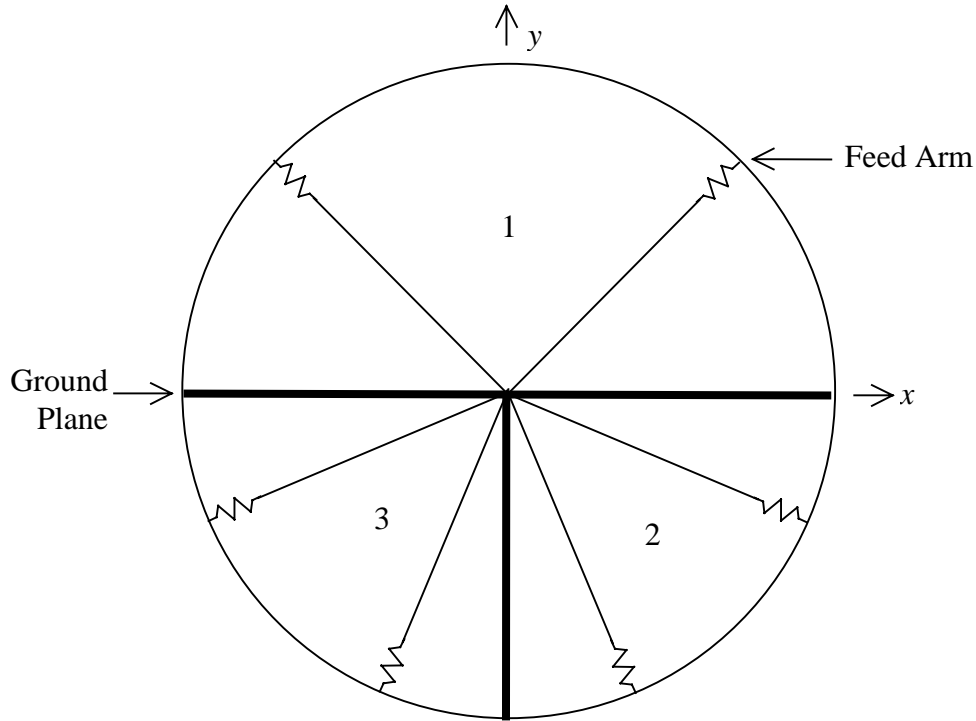
Figure 2.4. A tri-IRA consisting of a half-IRA and two quarter-IRAs. Channel 1 transmits V, and H and V can be constructed from the sum and difference of channels 2 and 3.

It is important to note that in the standard tri-IRA configuration of Figure 2.2, the two receive polarizations will have different sensitivities, in terms of volts. By symmetry, the sensitivity of the vertical receive signal (Channel 2 + Channel 3) is $1/\sqrt{3} = 57.7\%$ that of the horizontal receive signal (Channel 2 – Channel 3). In the Quad IRA of Figure 2.3, the sensitivities of the two receive polarizations are equal.

An important concept in the design of these antennas is symmetry, specifically the point symmetry groups (rotations and reflection) [5]. Here we consider N-fold rotations C_{Na} about the z-axis with N axial symmetry planes. The tri-IRA in Figure 2.2 is invariant to rotation by integer multiples of $2\pi/3$ (120º) and to reflections through the three axial symmetry planes defined by the three ground planes, or equivalently by the three bisecting planes for the three sectors. The quad-IRA in Figure 2.3 is invariant to rotation by integer multiples of $\pi/2$ (90º) and to reflections through the four axial symmetry planes, of which two are defined by the ground planes and two are defined by the two bisecting planes for the sectors. The tri-IRA with one half-IRA and two quarter-IRAs in Figure 2.4 does not have rotation symmetry but it does have reflection symmetry R_x, about the $x = 0$ plane (the y-z plane). It is the reflection symmetry that gives the isolation (in principle perfect) between the horizontal and vertical modes of operation. The vertical mode has symmetric fields with respect to the $x = 0$ plane, and the horizontal mode has antisymmetric fields with respect to this plane. The examples in Figures 2.2 and 2.3 have additional symmetry planes including the $y = 0$ plane (the x-z plane) with respect to which similar statements can be made.

III. Third-IRA Theory

We begin our discussion of theory with the third-IRA. We calculate the aperture fields, and then we optimize the impedance, according to various figures of merit, in the same sense as [6,7]. The modifications required to handle the quarter-IRA are handled in the next section.

The most critical calculation one must make with any IRA is its aperture height, h_a. This quantity is useful because the radiated field (dominant polarization on boresight) is described approximately as

$$E_{rad}(t) \approx \frac{h_a}{2\pi r c f_g} \frac{dV(t)}{dt} \tag{3.1}$$

where $V(t)$ is the exciting voltage on the feed arm and f_g is the feed impedance normalized to the impedance of free space. Furthermore, the received voltage is approximately

$$V_{rec}(t) \approx h_a \, E_{inc}(t) \tag{3.2}$$

where $V_{rec}(t)$ is the received voltage on the feed arms, and $E_{inc}(t)$ is the incident electric field on boresight. To calculate h_a, it is first necessary to find the fields and complex potential in the aperture.

To find the complex potential describing the aperture fields of a third-IRA, we have to establish a series of complex mappings from a half-IRA with a single feed arm to a third-IRA, as shown in Figure 3.1. The complex mapping that describes a half-IRA with a single feed arm (Figure 3.1A) is [6]

$$w_2(\zeta') = \text{arcsn}(-j\zeta'/m^{1/4}) \tag{3.3}$$

where $\zeta' = \zeta/a$, $\zeta = x + j\,y$, a is the aperture radius, and $w_2 = u_2 + j\,v_2$ is the complex potential. The complex mapping for a half-IRA with two feed arms is just the sum of this potential, rotated by $\pm 45^\circ$ (Figure 3.1B). Thus,

$$w_4(\zeta') = w_2(\zeta' e^{j\pi/4}) + w_2(\zeta' e^{-j\pi/4}) \tag{3.4}$$

To map a half-IRA into a third-IRA, one has to shrink ζ' into two-thirds the aperture area (Figure 3.1C). This is accomplished by replacing ζ' with $\zeta'^{3/2}$, resulting in the complex potential for the tri-IRA as

$$w_5(\zeta') = w_4(\zeta'^{3/2}) \tag{3.5}$$

Finally, we add a rotation of 30° to achieve reflection symmetry R_x, with respect to the $x=0$ plane (Figure 3.1D), and we find

$$w_6(\zeta') = w_5(\zeta' e^{-j\pi/6}) \tag{3.6}$$

This is the complex potential that describes the fields, and this is plotted in Figure 3.2 for a 100-ohm sector.
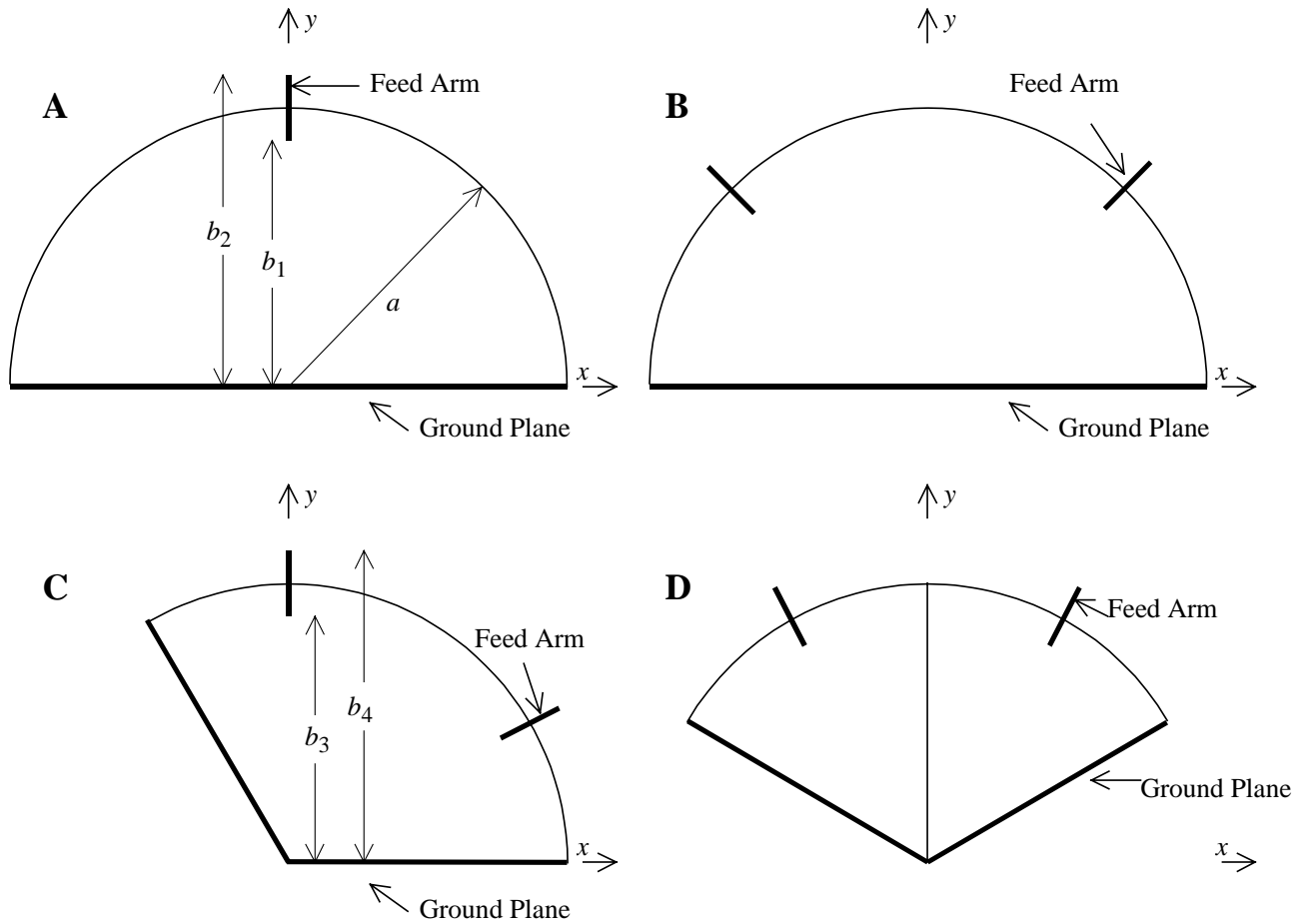
Figure 3.1. Progression of configurations mapping a half-IRA with a single arm (A), to a half-IRA with two arms (B), to a thrid-IRA (C), into a thrid-IRA with symmetry(D).

To calculate the characteristic impedance, we note that the impedance of the half-IRA with a single arm in Figure 3.1A is

$$f_{g,A} \;=\; \frac{1}{2}\frac{K(m)}{K(1-m)} \tag{3.7}$$

where $K(m)$ is the elliptic integral of the first kind, and m is calculated from

$$m = \left(\frac{b_1}{b_2}\right)^2, \qquad \frac{b_1}{a} = m^{1/4}, \qquad \frac{b_2}{a} = m^{-1/4} \tag{3.8}$$

By symmetry, the impedance of Figure 3.1B is just half of the above, or

$$f_{g,B} \;=\; \frac{1}{4}\frac{K(m)}{K(1-m)} \tag{3.9}$$

The impedance of the third-IRAs in Figures 3.1C and 3.1D are just the same as above, but m is calculated instead from
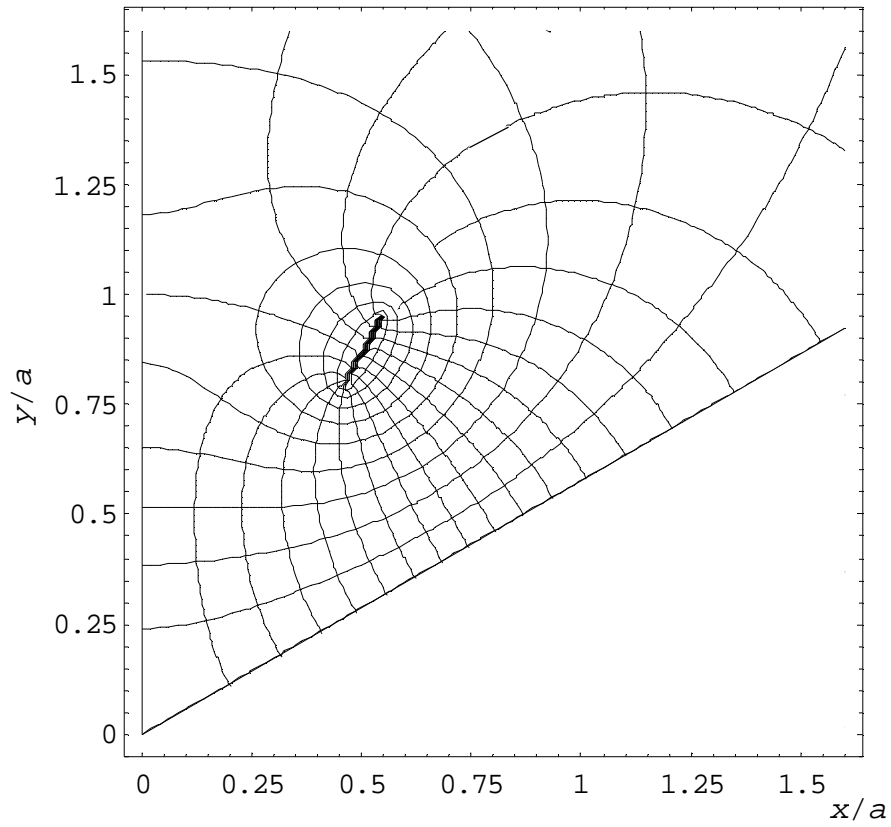
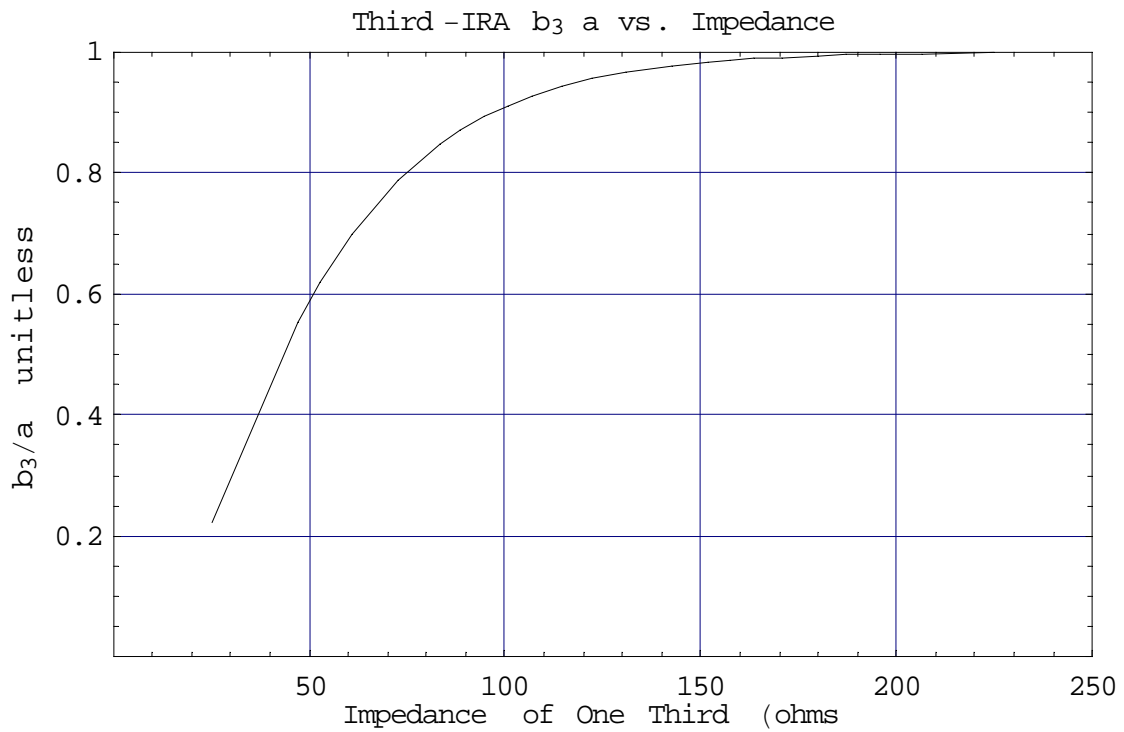Figure 3.2. Complex potential associated with a third-IRA of 100-ohm impedance.

Figure 3.3. The ratio b_3/a as a function of impedance of a third-IRA.

$$m = \left(\frac{b_3}{b_4}\right)^3, \qquad \frac{b_3}{a} = \left(\frac{b_1}{a}\right)^{2/3} = m^{1/6}, \qquad \frac{b_4}{a} = \left(\frac{b_2}{a}\right)^{2/3} = m^{-1/6} \qquad (3.10)$$

Using these expressions, we can plot impedance as a function of b_3. This is shown in Figure 3.3. Note that we can find b_4/a from b_3/a using $b_4/a = 1/(b_3/a)$.

To convert the above locations in the aperture plane to angles from the focus, we use the standard stereographic transformation $\Psi = 2 F \tan(\theta/2)$ [2]. In this equation, Ψ is the radius in the aperture plane, and $\Psi = |\zeta|$. Furthermore, θ is the angle from the focal point, and F is the focal length. The angle from the x-axis, ϕ, remains unchanged.

Now that we have the field lines, we can calculate the aperture height, h_a, which is expressed as

$$h_a = \frac{f_g}{V_o} \iint_{S_a} E_y \, dx \, dy \qquad (3.11)$$

where S_a is the surface containing the aperture, and C_a is the contour around the aperture. This integral is calculated from by a contour around half of the aperture, C_a', as shown in Figure 3.4. This is calculated as [8]

$$h_{a_y} = -\frac{2}{\Delta v} \oint_{C_a'} v(y) \, dy = -\frac{2}{\Delta v} \oint_{C_a'} u(x) \, dx \qquad (3.12)$$

In this case, it is simplest to use the expression with $u(x)$, because along the ground plane, I_1, $u(x) = 0$. Furthermore, along the left-right plane of symmetry, I_3, $dx = 0$. This leaves only the integral along the arc, I_2. This is calculated numerically in one continuous integral, from the ground plane to the plane of symmetry. The small diversion around the conductor makes no contribution to the integral, because $u(x)$ is a constant on the conductor. Note also that $u(x)$ is continuous along the arc as it passes through the conductor.
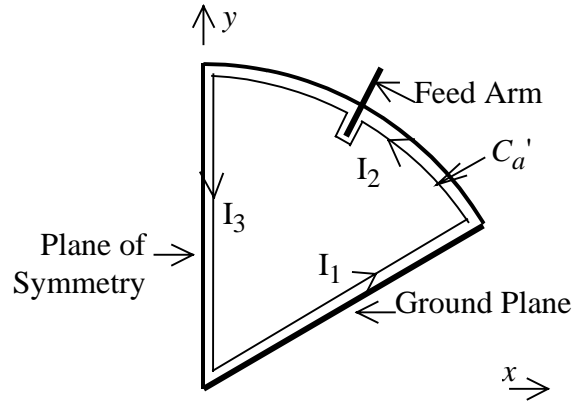

Figure 3.4. The contour around half of the aperture, C_a'.

We can plot h_a as a function of impedance, and this is shown in Figure 3.5. This is the essential data we need in order to predict performance of the antenna as built. Note that the antenna we built has an impedance of 80 ohms in each sector, so we expect a $h_a/a = 0.234$.
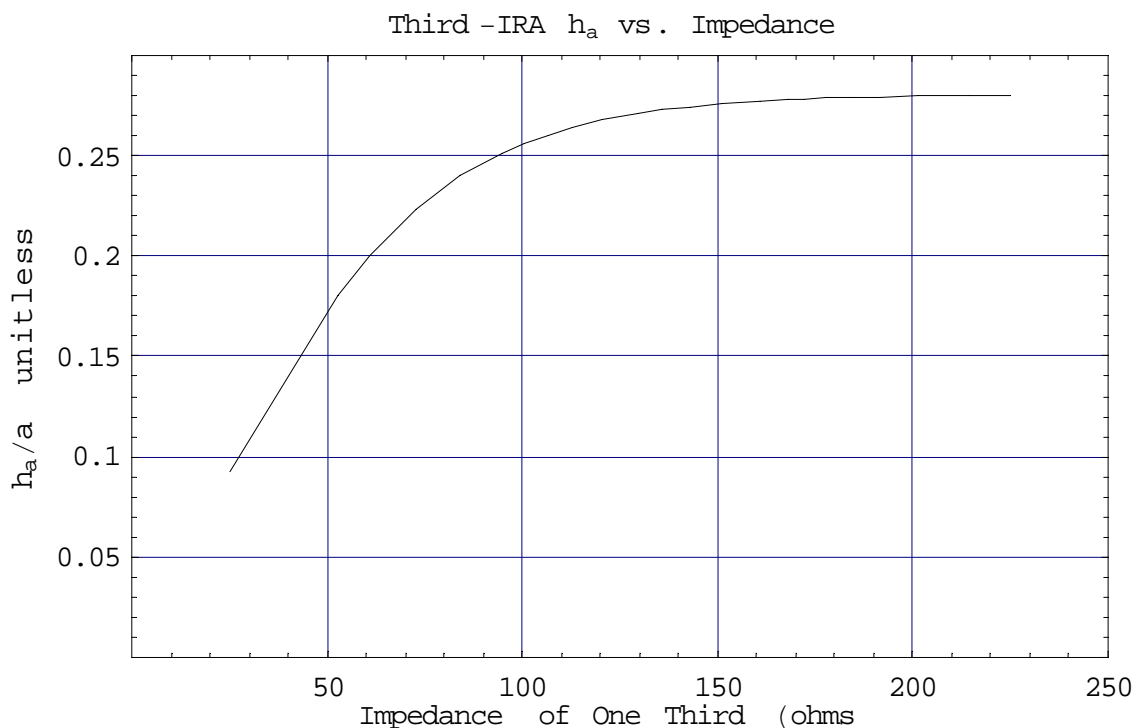

Figure 3.5. The aperture height, h_a, of a third-IRA, as a function of impedance.

There are various figures of merit one can use to optimize the impedance [6,7,9,10]. First, we consider a figure of merit that is power-based, and is independent of the feed cable impedance. We denote this as η_1, and it is defined as

$$\eta_1 = \frac{h_a}{\sqrt{f_g}} \tag{3.13}$$

This is plotted in Figure 3.6, where we see a peak near 78 ohms.

Another figure of merit we can use assumes that the antenna is fed by a 50 Ω cable [10]. In this case, the figure of merit is

$$\eta_2 = \frac{\tau_p h_a}{\sqrt{f_g}} \, , \qquad \tau_p = \frac{2\sqrt{Z_{feed} Z_{cable}}}{Z_{feed} + Z_{cable}} \, , \qquad Z_{feed} = Z_o f_g \tag{3.14}$$

where τ_p is the square-root power transmission coefficient from a 50 Ω cable to the TEM feed. Furthermore, $Z_o = 376.727 \, \Omega$ and Z_{cable} is 50 Ω. In cases where no balun is used, this is probably the most meaningful figure of merit. This quantity is plotted for the third-IRA in Figure 3.6. Here, we see a peak near 71 ohms. This tends to suggest that we would like to build

the antenna with an impedance of 71 ohms, but the feed arms become prohibitively wide with at impedances below 80 Ω.
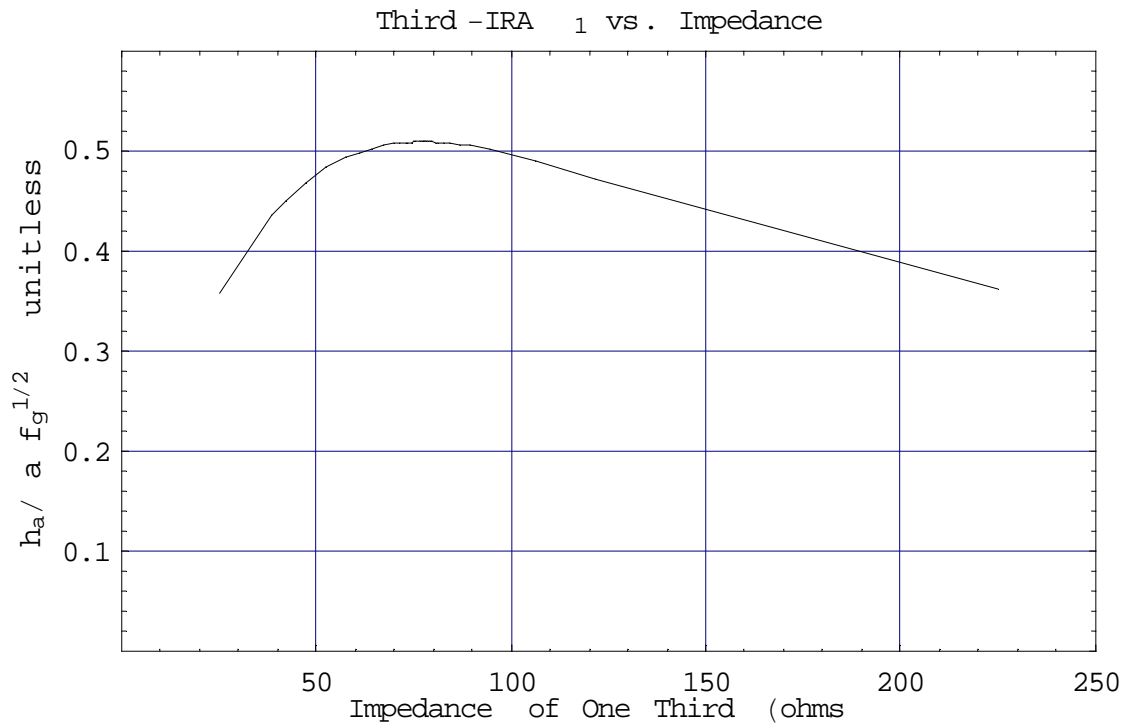
Third $-$IRA η_1 vs. Impedance

Figure 3.6. The figure of merit η_1 as a function of impedance for a third-IRA.
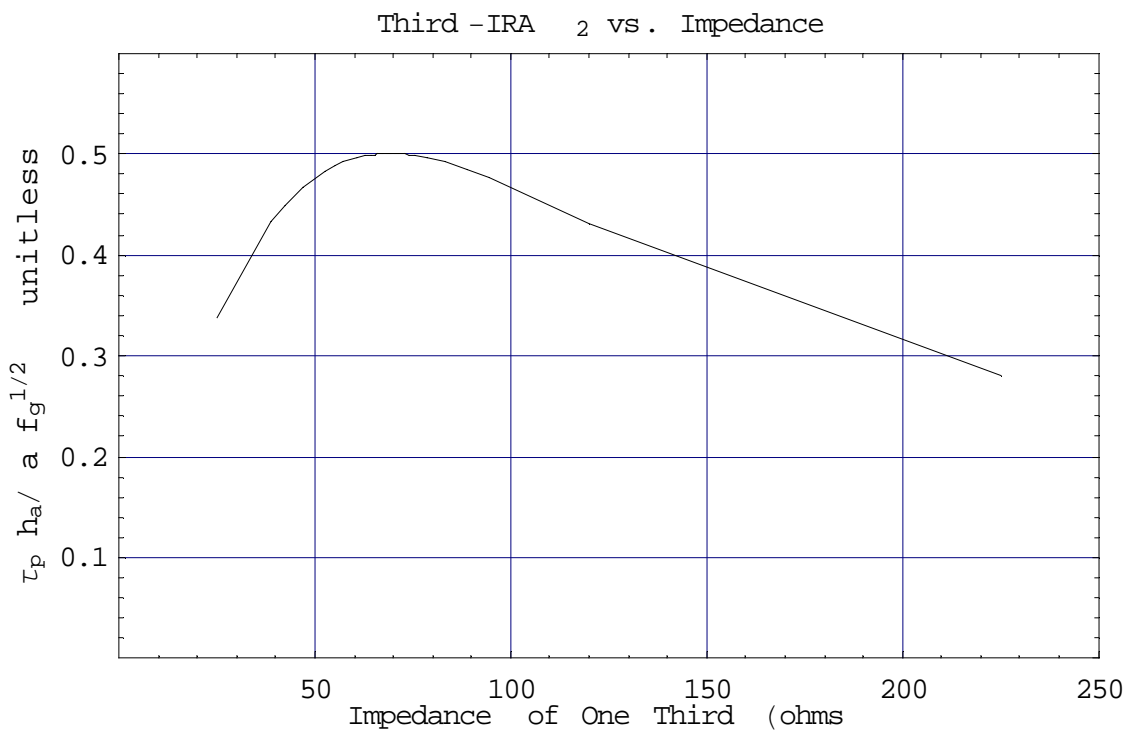
Third $-$IRA η_2 vs. Impedance

Figure 3.7. The figure of merit η_2 as a function of impedance for a third-IRA.

Finally, we consider a figure of merit based on voltage. In other words, assume that the limiting consideration for a high-voltage transmitting antenna is the peak voltage sustainable before breakdown. Under this constraint, one wants to optimize η_3, which is defined as

$$\eta_3 = \frac{h_a}{f_g} \tag{3.15}$$

We plot this figure of merit for the third-IRA as a function of impedance in Figure 3.8. In this case, the figure of merit is optimal at very low impedances, approaching zero ohms. This is a non-physical result, because it does not take into account feed blockage.
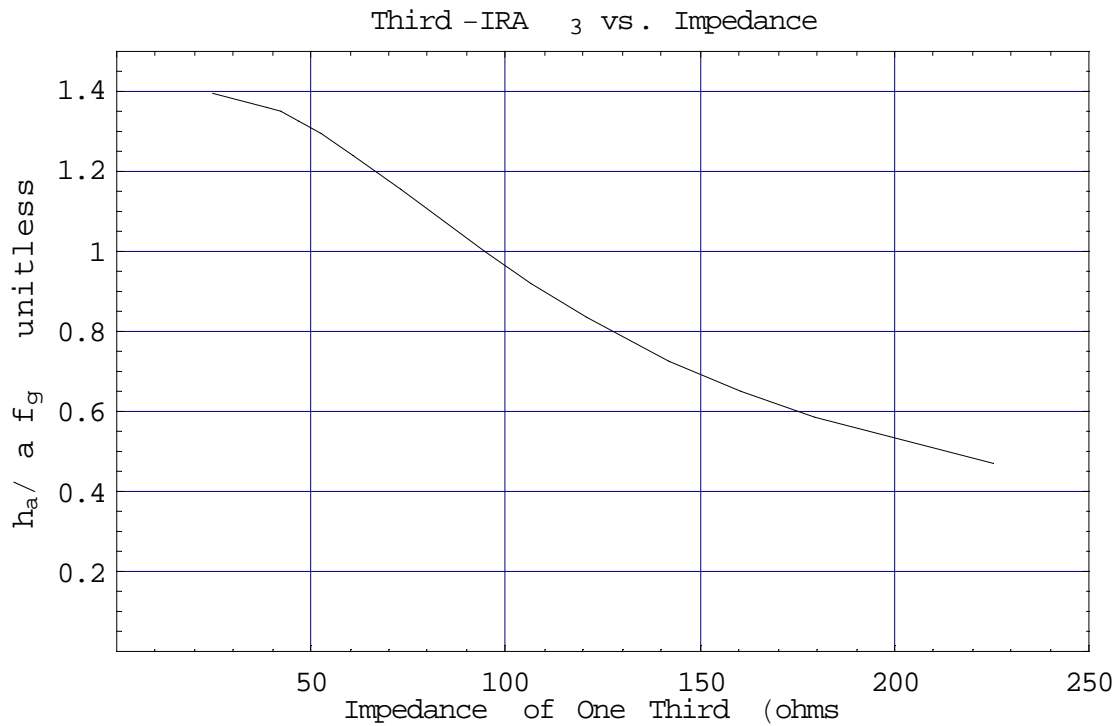
Figure 3.8. The figure of merit η_3 as a function of impedance for a third-IRA.

IV. Quarter-IRA Theory

We consider next the theory describing a quarter-IRA. It turns out that this theory is a minor modification of the theory used to describe the third-IRA of the previous section.

First, we consider the complex mapping required to calculate the electric fields in the aperture. Again, starting from a Half-IRA with a single feed arm, we map to a Half-IRA with two feed arms, as shown in Figure 4.1A and 4.1B. The complex potential describing the Half-IRA with two feed arms is $w_4(\zeta')$, as defined previously in (3.4). To map to a quarter-IRA with two feed arms (Figure 4.1E), we have to replace ζ' with ζ'^2, resulting in

$$w_7(\zeta') = w_4(\zeta'^2) \tag{4.1}$$

We achieve reflection symmetry by rotating the map by $\pi/4$, resulting in (Figure 4.1F)

$$w_8(\zeta') = w_7(\zeta' e^{-j\pi/4}) \tag{4.2}$$

This is the complex potential describing a quarter-IRA. A mapping is shown in Figure 4.2 for an impedance of 100 ohms.
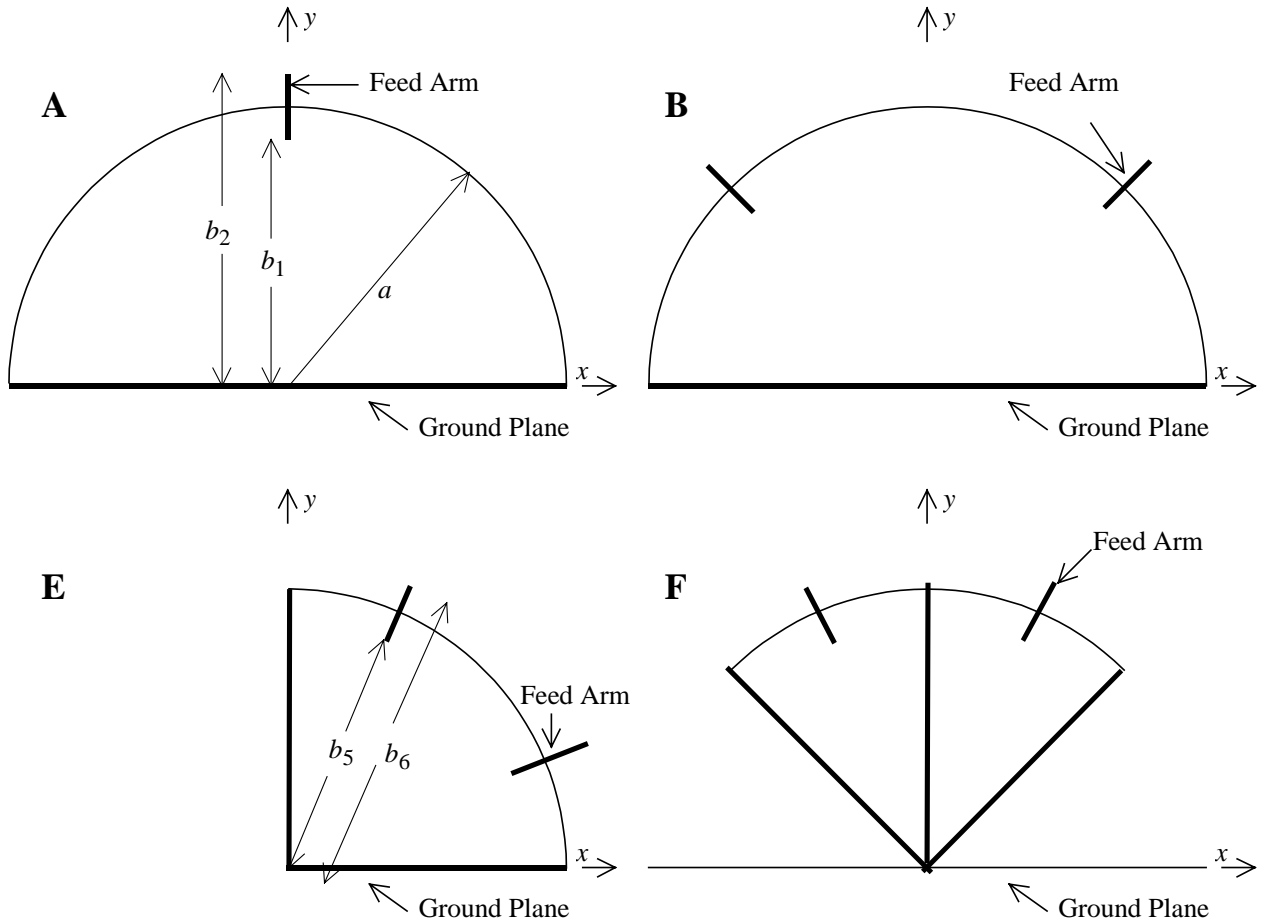

Figure 4.1. Progression of configurations mapping a half IRA with a single arm (A), to a half IRA with two arms (B), to a quarter-IRA (E), into a quarter-IRA with symmetry(F).
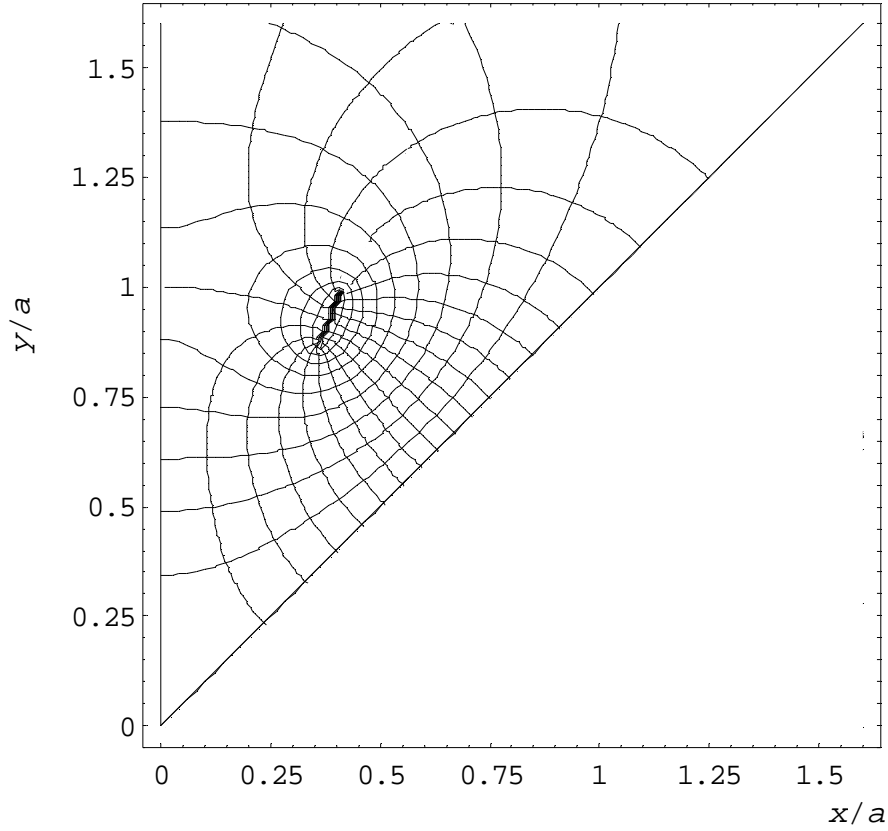
13

Figure 4.2 Complex mapping of the quarter-IRA, with an impedance of 100 ohms.

To find the impedance of a quarter-IRA, we once again use (3.9), or

$$f_g \quad = \quad \frac{1}{4} \frac{K(m)}{K(1-m)} \tag{3.9}$$

with the modification that m is defined by

$$m = \left(\frac{b_5}{b_6}\right)^4, \qquad \frac{b_5}{a} = \left(\frac{b_1}{a}\right)^{1/2} = m^{1/8}, \qquad \frac{b_4}{a} = \left(\frac{b_2}{a}\right)^{1/2} = m^{-1/8} \tag{3.10}$$

where b_5 and b_6 are the inner and outer radius of the conductor as projected into the aperture plane, as shown in Figure 4.1E. A plot of b_5/a as a function of impedance is shown in Figure 4.3.

It is now straightforward to calculate the aperture height and the two figures of merit, η_1 and η_2, as defined in the previous section. The aperture height, h_a, is plotted in Figure 4.4. The figure of merit η_1 is plotted in Figure 4.5, and it has a maximum near 79 ohms. The figure of merit η_2 is plotted in Figure 4.6, and it has a maximum near 69 ohms. The figure of merit η_3 is plotted in Figure 4.7, and it has an optimum at zero ohms. This last result is non-physical due to feed blockage.
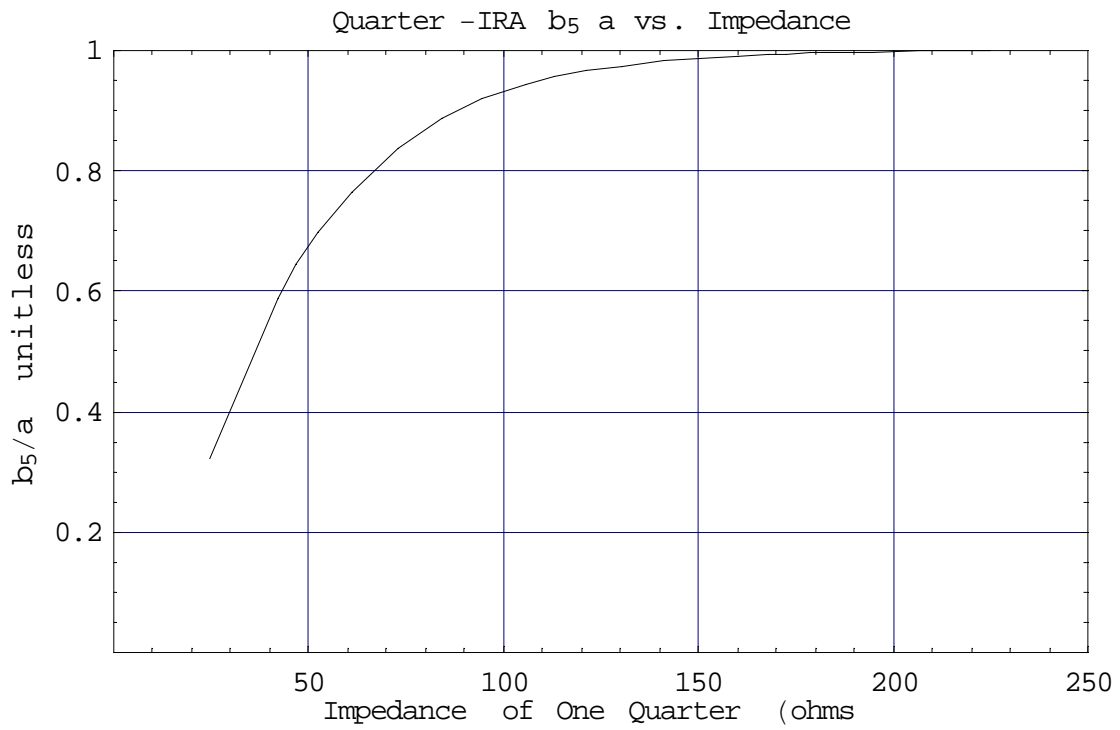
14

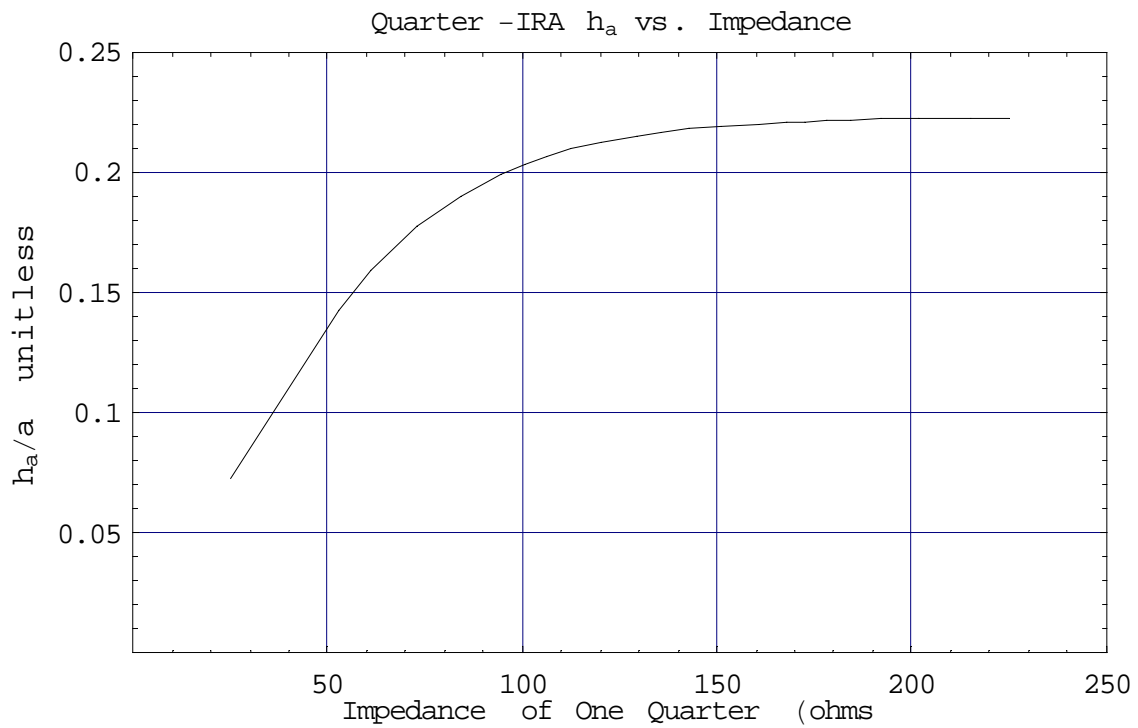Figure 4.3. The ratio b_5/a as a function of impedance for a quarter-IRA.

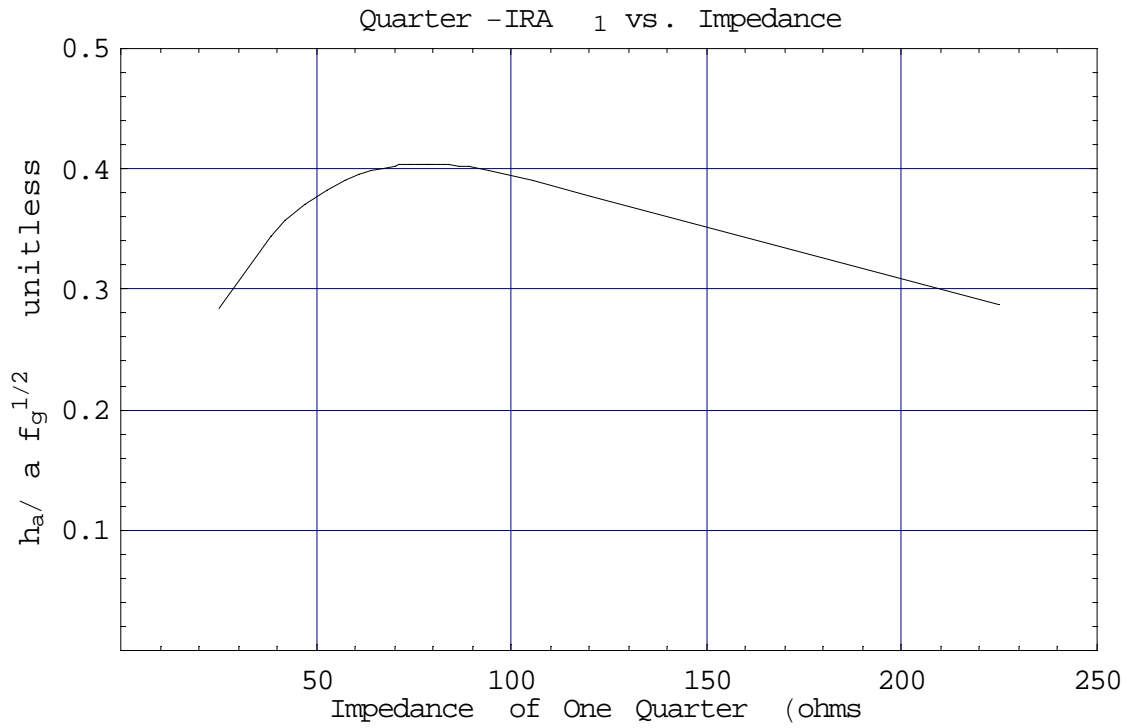Figure 4.4. The aperture height, h_a, of a quarter-IRA, as a function of impedance.

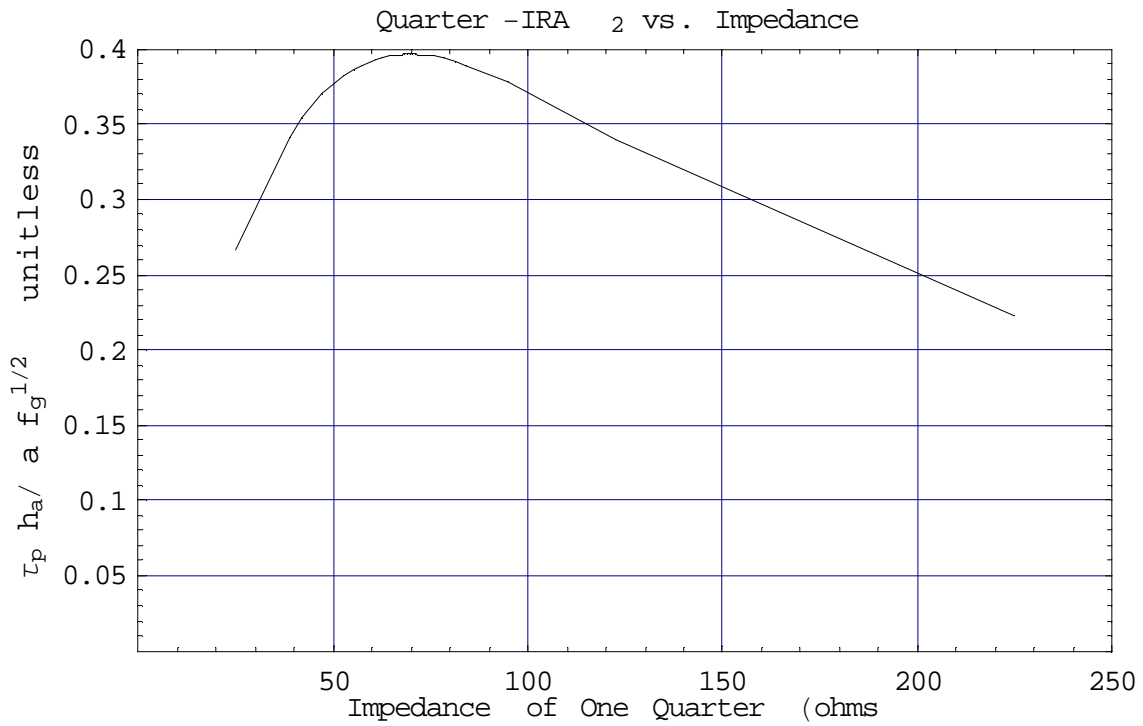Figure 4.5. The figure of merit, η_1, as a function of impedance for a quarter-IRA.

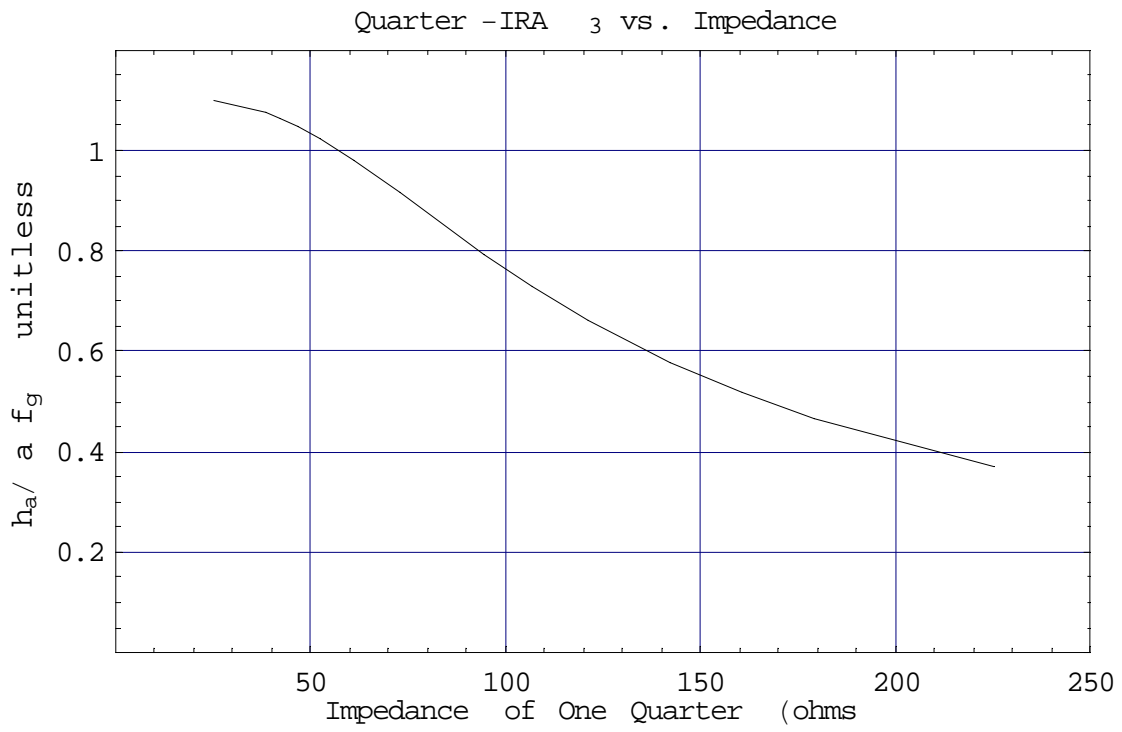Figure 4.6. The figure of merit, η_2, as a function of impedance for a quarter-IRA.

Figure 4.7. The figure of merit, η_3, as a function of impedance for a quarter-IRA.

V. Tri-IRA Measurements

In order to test our theory, we designed, built, and tested a tri-IRA. We consider here first the design features of the tri-IRA, and then describe the testing. Diagrams of the tri-IRA are shown in Figure 5.1 and 5.2, and two photographs are shown in Figure 5.3.

The design was based on an inexpensive reflector from Metal Spinners. This reflector is a 36-inch diameter aluminum parabolic dish with a focal length of $F = 13.4$ inches, and an F/D ratio of 0.37. The design split the dish into 3 equal sectors, one for transmit and the other two for receive. The two feed arms in each sector are supported by 0.5-inch diameter Teflon rods. Each feed arm is terminated with three 480 Ω resistors in parallel. These resistors, from HVR, are miniature versions of the bulk ceramic resistors used on the larger antennas, and they can withstand about 6 kV. Each sector of the tri-IRA has an impedance of 80 Ω. Semi-rigid 50 Ω coaxial cables are used for the feeds between the connector box and the feed point in each of the three sectors of the antenna. The cables are attached to the ground planes with conductive epoxy.

The first tests of the tri-IRA were TDRs of each sector, one of which is shown in Figure 5.4. All three TDRs were very similar. Next, we measured the radiation patterns of the three sectors. Both the vertical and horizontal E field patterns for each of the three sectors were measured in the E and H planes. These measurements were made using the PSPL 4015C pulser and the Tektronix 11801B oscilloscope. The sensor was a Farr Research Model FRI-TEM-01-100, which is a 100 Ω TEM horn sensor. The measurements were made at 5° increments from –25° to +25° in both the E and H planes as measured from the axis of the antenna. The measured fields of Sector 1 are shown in Figure 5.5. The half power points (based on raw voltage) in the H plane occur at ±2°and in the E plane at ±5°. Future antennas of this type will be designed to have a broader beam width, to have an increased look angle.

Next, we converted the corrected measured field on boresight to the antenna's impulse response, $h(t)$. This is shown in Figure 5.6 (top), and its integral is shown on the bottom. The antenna's h_a is the area under the impulse, and this is normally determined from the jump in the integral. From Figure 5.6, we estimate the jump in the integral to be about 9.0 cm. Recall from Figure 3.5 that we expect $h_a/a = 0.234$ for an 80-ohm sector, and $a = 18$ in (45.7 cm). Thus, for our antenna we expect $h_a = 10.7$ cm and we measured 9.0 cm. So **our measured results are 84% of the theoretical results.** This is very good agreement. The discrepancy is due to cable losses and aperture blockage.

Finally, we tested the antenna in radar mode. For this, we placed an aluminum sheet, 32" x 38", nine feet in front of the tri-IRA. The reflector was sitting on the ground, and was oriented such that it would reflect signal directly back into the antenna. While driving Channel 1 of the tri-IRA with the Kentech source, we measured the returned waveform on Channel 2 with an SCD5000. The Kentech pulser has a 1.5 kV peak output with a 240 ps risetime, and adjustable pulse width. This was done with both the sheet present, and with the antenna pointed up into the air (an air shot), and the results are shown in Figure 5.7. The effect of the reflector is a clear bump in the data. It must be noted, however, that the noise in the air shot is of the same order of magnitude as the reflected signal, so it will be important to reduce this noise in later designs. This is discussed further in the next section.
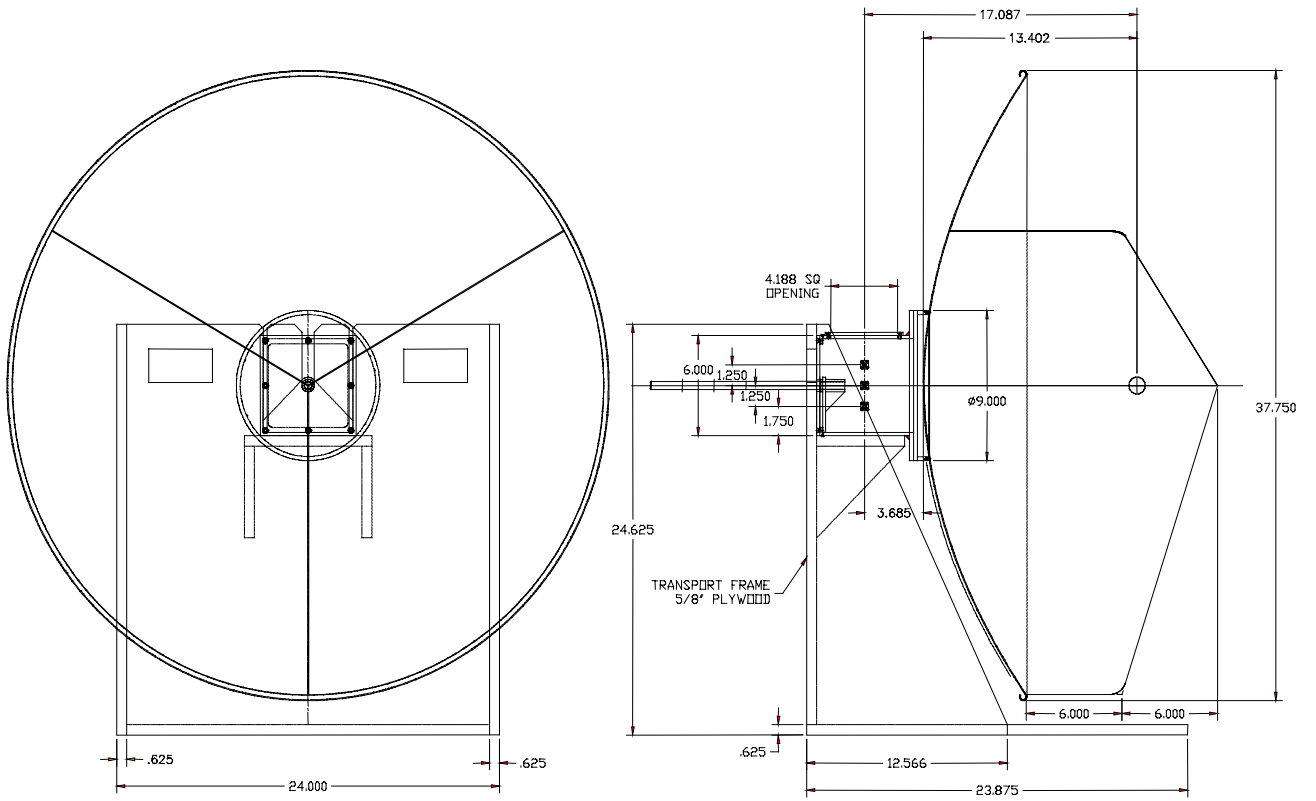
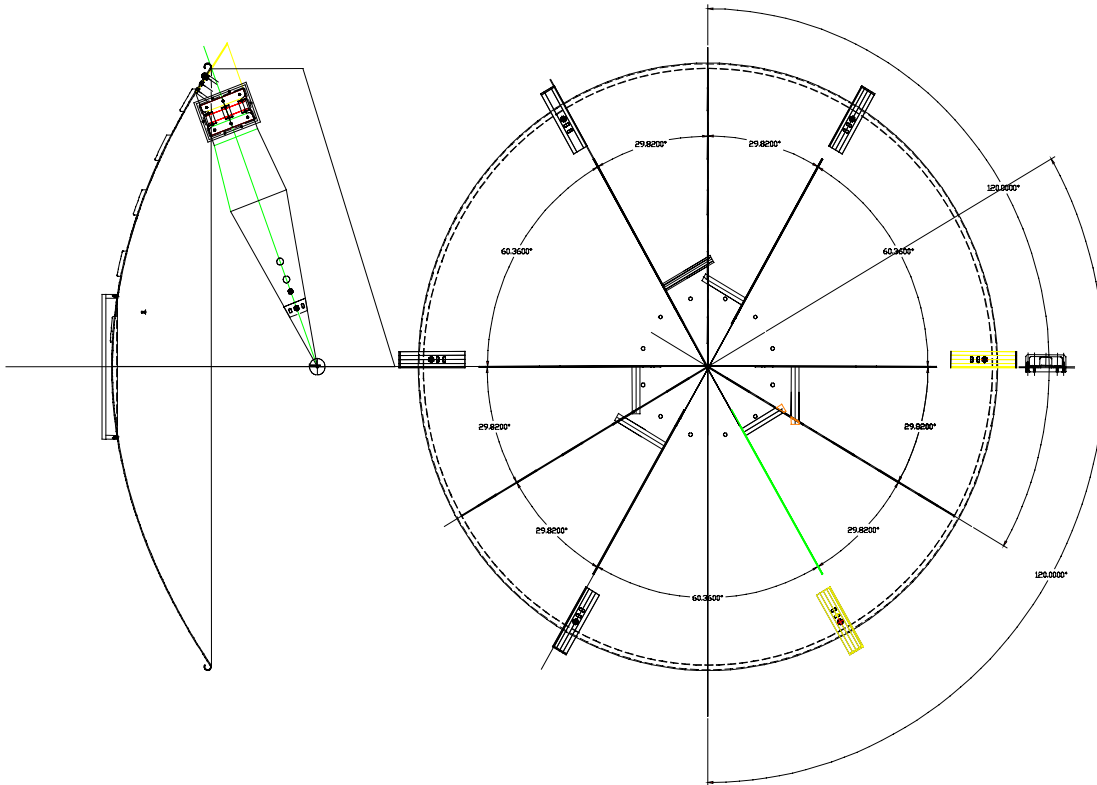Figure 5.1. The tri-IRA on storage and transportation stand without feed elements.

Figure 5.2 View of the tri-IRA showing feed elements.

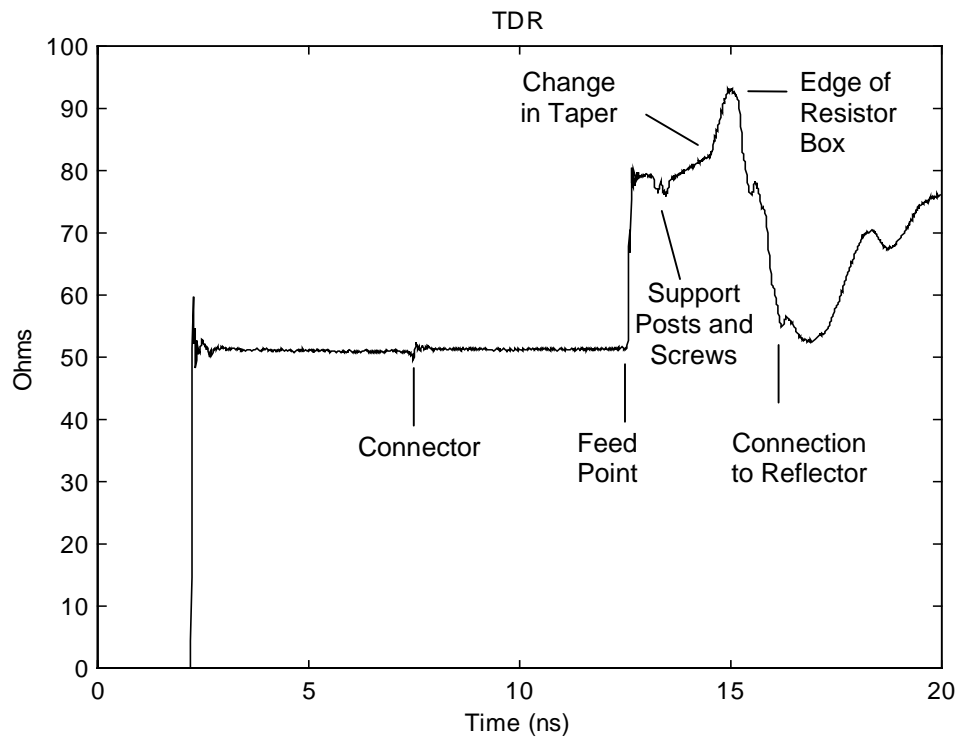Figure 5.3. The tri-IRA, from front and side perspectives.

Figure 5.4. TDR of Sector 1.

Tri-IRA Sector 1, E-Plane Scan, 16.6m

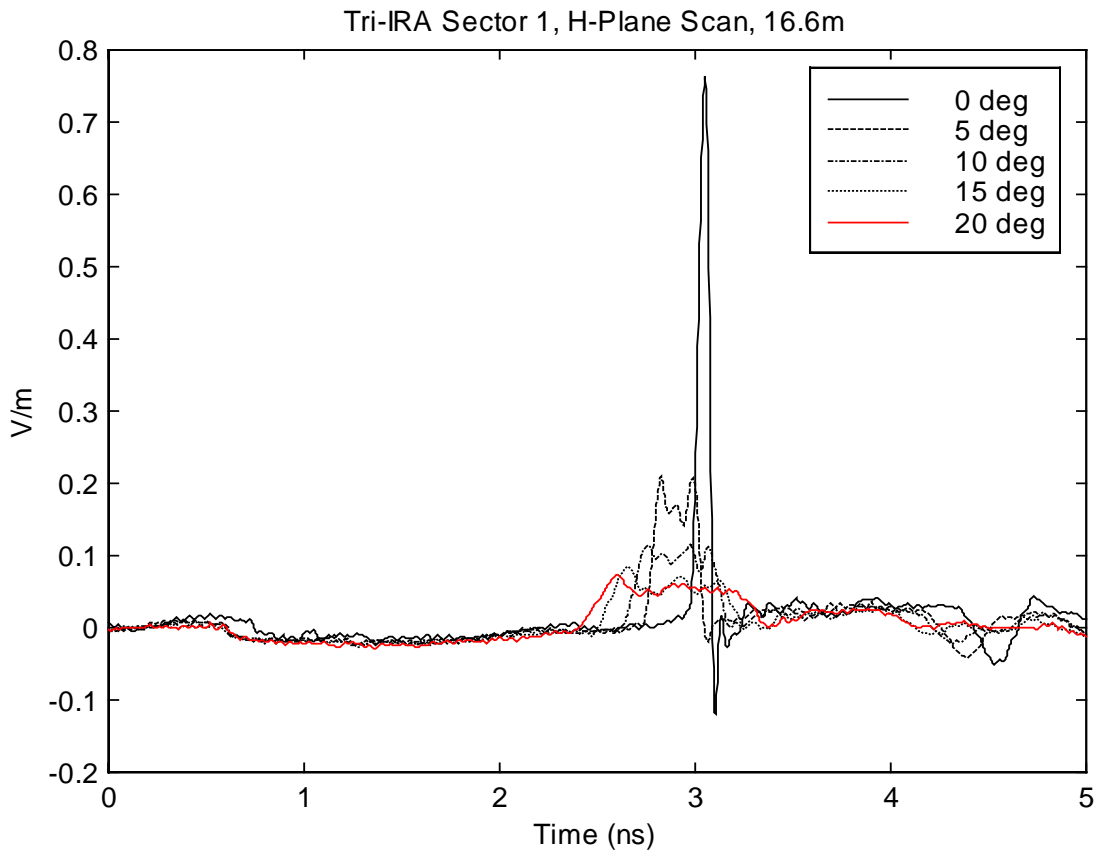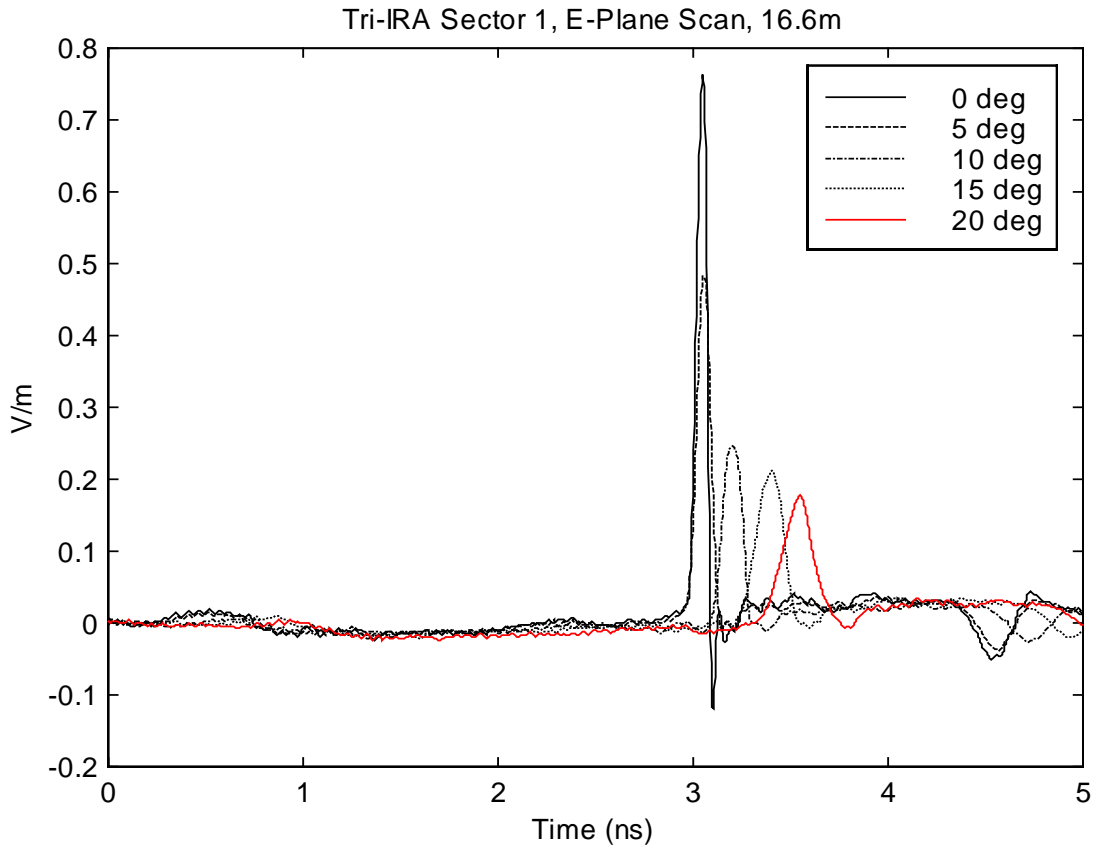**Tri-IRA Sector 1, H-Plane Scan, 16.6m**

Figure 5.5. Sector 1, Vertical Polarization, E-Plane (top) and H-Plane (bottom) scans at 16.6 m.

Impulse Response, Tri-IRA
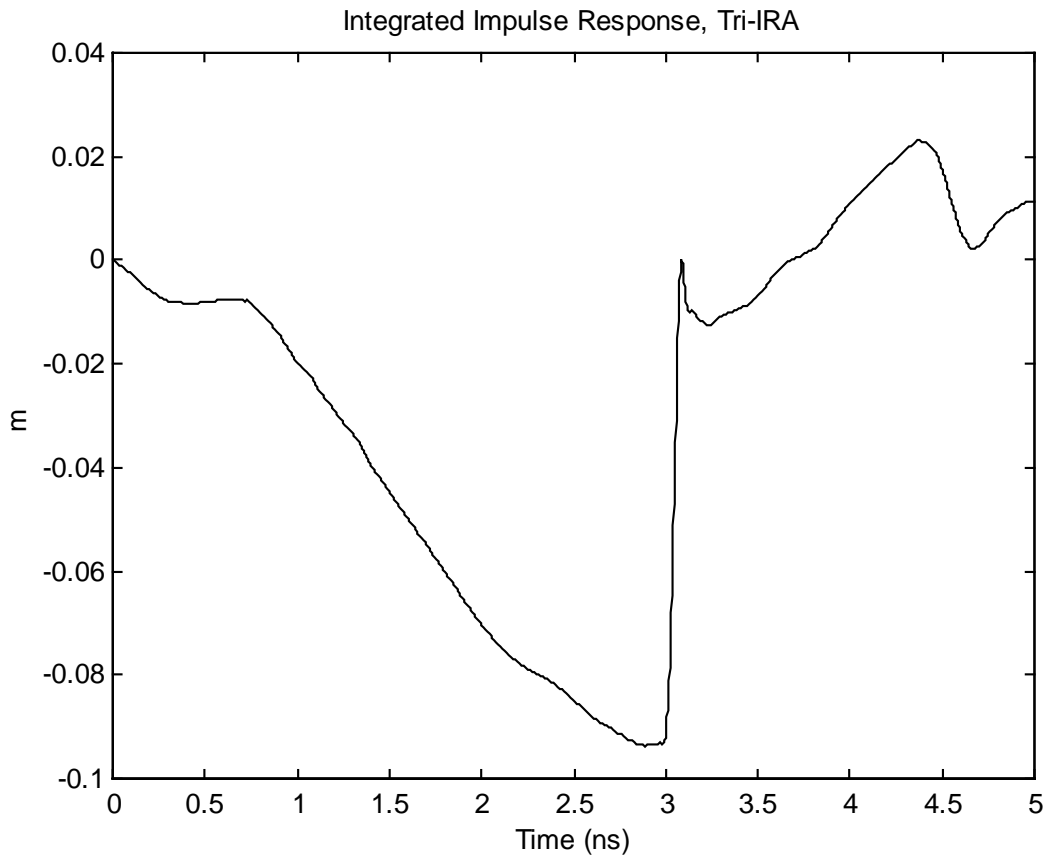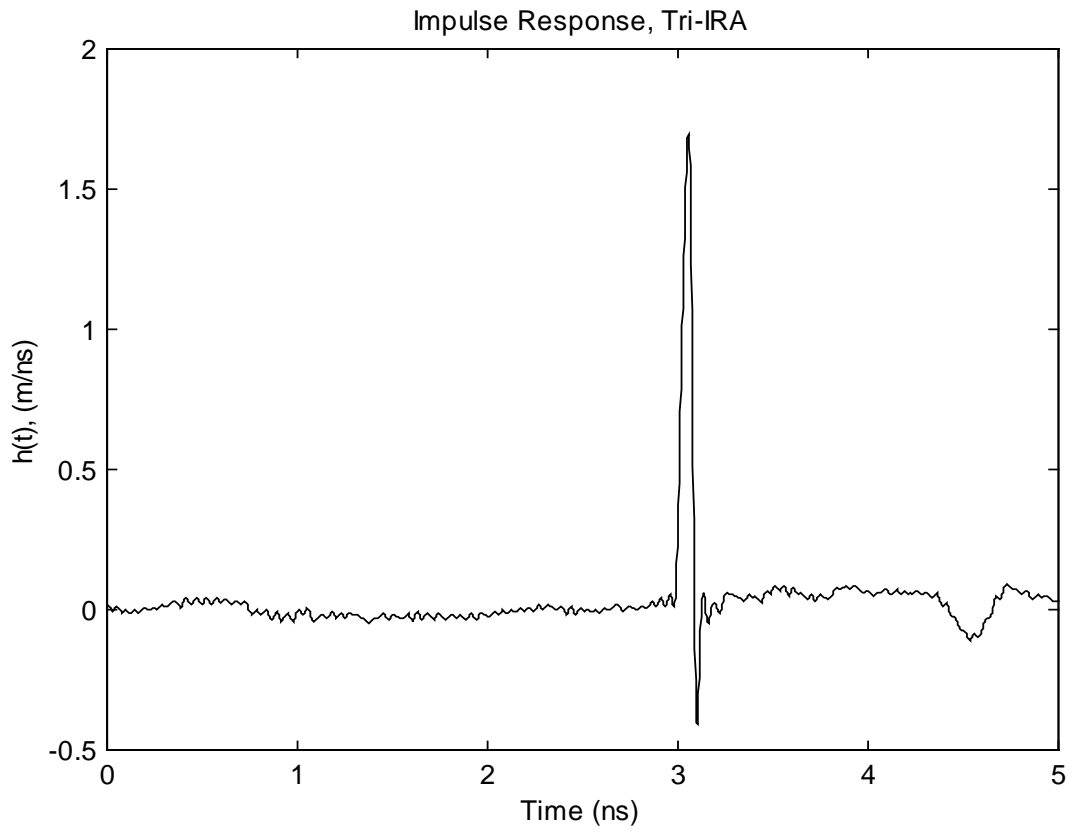

Integrated Impulse Response, Tri-IRA

Figure 5.6 Impulse response of the tri-IRA, top, and its integral, bottom.
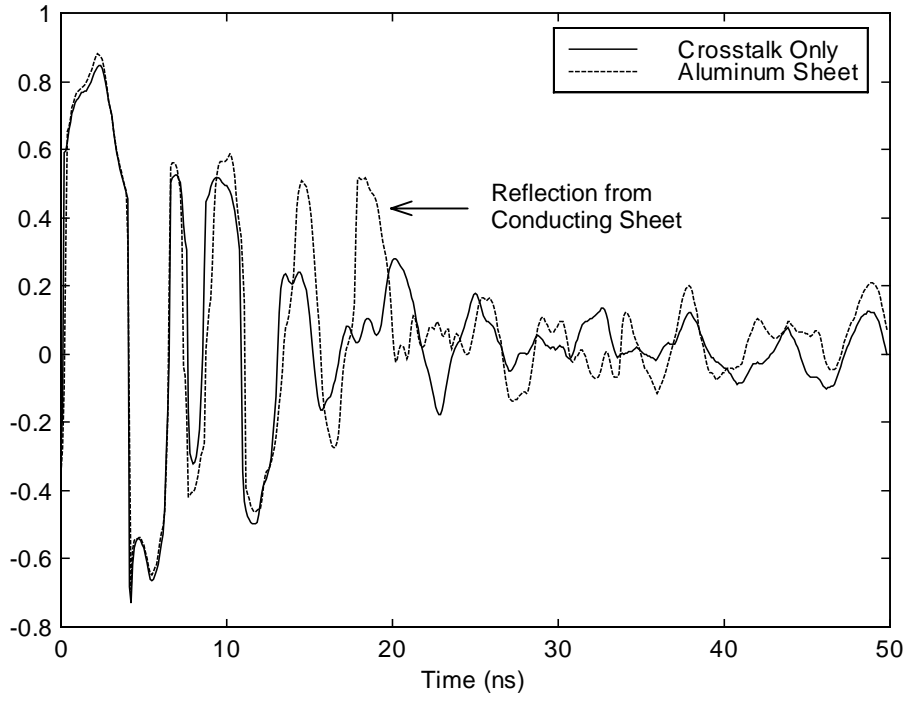
Figure 5.7. The reflection from an aluminum sheet, overlaid with an air shot (crosstalk).

VI. Discussion

The radar mode data provided in Figure 5.7 indicate to us a number of modifications that will be necessary in the next version of the antenna and radar system. There is a substantial noise signal at late times which is superimposed upon the radar measurement. This late-time noise can be subtracted off the measured signal, but it is easier to handle if it is smaller.

There are several sources of late-time noise. First, there is crosstalk from the transmit to receive channels. One might expect crosstalk to occur only at early times, so it should be possible to time-gate it out. But the antenna is not matched to the 50 Ω feed lines, either on the transmit or receive channels. This leads to multiple reflections on both transmit and receive channels, so the crosstalk persists into late time. Note also that the limiter used on the receive channel also has some reflections, and the Kentech source may have reflections as well.

To reduce late-time noise, one must consider both matching the antenna better to 50 Ω and reducing the crosstalk. One can reduce the crosstalk in the present design by increasing the size of the ground planes, and by using anechoic and resistive materials between the antenna channels. However, obtaining a better match of the antenna to 50 Ω is more challenging. One might match the tri-IRA by using a 75 Ω feed, and using a 75 Ω feed cable. Then, at the junction of the 50 Ω and 75 Ω circuitry, one could add a resistor matching network, an example of which is shown in Figure 6.1. Note that this circuit works equally well in both directions. Alternatively, one could explore using other types of antennas, such as TEM horns with terminations. These have less gain than IRAs, but having a clean signal may be a higher priority than having an optimal antenna gain. In the measurements presented here, we have plenty of signal. We plan to address these issues and tradeoffs in future work.
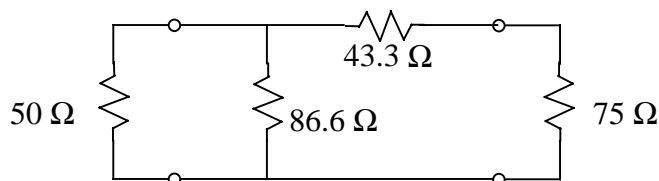

Figure 6.1.   A circuit for matching 50 Ω into 75 Ω, and 75 Ω into 50 Ω .

VII. Conclusion

We have described here a class of very compact antennas that are useful in searching for manmade objects using polarization diversity. We have optimized the impedance, and we have built a prototype tri-IRA. The measured radiated field on boresight is predicted well by our theory. When operated in radar mode, this antenna exhibited some late-time crosstalk from one channel to the next. Thus, the next step in this research will be to reduce crosstalk by increasing the ground plane size and by application of resistive and absorbing materials. It will also be necessary to reduce late-time reflections due to mismatches in both the transmit and receive circuits.

Patent Notice

A preliminary patent application is pending on the work described in this note.

References

1. C. E. Baum, Symmetry in Electromagnetic Scattering as a Target Discriminant, Interaction Note 523, October 1996.

2. C. E. Baum and E. G. Farr, Impulse Radiating Antennas, in H. L. Bertoni *et al* (eds.), *Ultra-Wideband, Short-Pulse Electromagnetics*, New York, Plenum, 1993.

3. E. G. Farr, C. E. Baum, and C. J. Buchenauer, Impulse Radiating Antennas, Part II, pp. 159-170 in L. Carin and L. B. Felsen (eds.) *Ultra-Wideband, Short-Pulse Electromagnetics 2*, New York, Plenum Press, 1995.

4. E. G. Farr and C. E. Baum, Impulse Radiating Antennas, Part III, pp. 43-56 in C. E. Baum, L. Carin and A. P. Stone (eds.) *Ultra-Wideband, Short-Pulse Electromagnetics 3*, New York, Plenum, 1997

5. C. E. Baum and H. N. Kritikos, *Electromagnetic Symmetry*, Taylor and Francis, 1995.

6. E. G. Farr, Optimizing the Feed Impedance of Impulse Radiating Antennas, Part I: Reflector IRAs, Sensor and Simulation Note 354, January 1993.

7. E. G. Farr, Optimization of the Feed Impedance of Impulse radiating Antennas, Part II: TEM Horns and Lens IRAs, Sensor and Simulation Note 384, November 1995.

8. C. E. Baum, Aperture Efficiencies for IRAs, Sensor and Simulation Note 328, June 1991.

9. E. G. Farr and C. E. Baum, Extending the Definitions of Antenna Gain and Radiation Pattern Into the Time Domain, Sensor and Simulation Note 350, November 1992.

10. E. G. Farr and C. E. Baum, Time Domain Characterization of Antennas with TEM Feeds, Sensor and Simulation Note 426, October 1998.